International Journal of Naval Architecture and Ocean Engineering 11 (2019) 70–81

Contents lists available at ScienceDirect

International Journal of Naval Architecture and Ocean Engineering

journal homepage: http://www.journals.elsevier.com/international-journal-of-naval-architecture-and-ocean-engineering/

An improved Rankine source panel method for three dimensional water wave problems

Aichun Feng [a, *], Yunxiang You [b, c], Huayang Cai [d]

[a] Department of Civil and Environmental Engineering, National University of Singapore, Kent Ridge, Singapore, 117576, Singapore
[b] State Key Laboratory of Ocean Engineering, Shanghai Jiao Tong University, Shanghai 200240, China
[c] Collaborative Innovation Center for Advanced Ship and Deep-Sea Exploration, Shanghai 200240, China
[d] Institute of Estuarine and Coastal Research, School of Marine Sciences, Sun Yat-sen University, Guangzhou 510275, China

ARTICLE INFO

Article history:
Received 16 August 2017
Received in revised form
20 January 2018
Accepted 5 February 2018
Available online 24 February 2018

Keywords:
Continuous source panel
Free surface source distribution
Water wave problem

ABSTRACT

An improved three dimensional Rankine source method is developed to solve numerically water wave problems in time domain. The free surface and body surface are both represented by continuous panels rather than a discretization by isolated points. The integral of Rankine source $1/r$ on free surface panel is calculated analytically instead of numerical approximation. Due to the exact algorithm of Rankine source integral applied on the free surface and body surface, a space increment free surface source distribution method is developed and much smaller amount of source panels are required to cover the fluid domain surface than other numerical approximation methods. The proposed method shows a higher accuracy and efficiency compared to other numerical methods for various water wave problems.

1. Introduction

Accurate estimations of wave loads and responses of floating structures are of practical importance in offshore engineering field. This wave-body interaction problem within a potential flow framework, can be solved numerically based on either a free surface Green function or a Rankine source approach. The former model involves a complicated free surface Green function which requires a singular wave integral on the free surface boundary (see Wehausen and Laitone (1960)). The latter model only needs to calculate the integral of Rankine sources on free surface and body boundaries and it works as a very efficient model in time domain since only a simple Green function is required to calculate.

One key numerical technique in the boundary integral method is the evaluation of Rankine source on the surface panel. The fluid surface can be discretized by a B-Spline function into curve panels (Nakos and Sclavounos, 1990; Maniar, 1995; Lee et al., 1996). After the surface discretization, one popular method to calculate Rankine source integral is Gaussian quadrature numerical integration (Isaacson and Cheung, 1991; Kouh and Suen, 2001; Gao and Zou, 2008; Das and Cheung, 2012; Bai and Teng, 2013). This method introduces weight functions and associated polynomials to approximate the Rankine source integral. However this method is only valid when the source points and control points are not in the same panel. It is troublesome as singularity integral arises when these two kinds of points are located closely in the same panel. Yonghui and Xinsen (1988); Eatock Taylor and Chau (1992) introduced a triangular polar-coordinate to map the sub-element to a unit square and this transformation allows the Gaussian integration valid on the square. As a numerical approximation, in order to get higher accuracy, more Gaussian sampling points are needed and this significantly increases the computational loads.

The analytical expression of Rankine source integral was first derived by (Hess and Smith, 1964) for arbitrary bodies in unbounded fluid domains. By using constant-strength distributions on quadrilateral flat panels, the panel integral can be analytically expressed as a superposition of integral over four parallel strips. Each strip is defined by one side of the quadrilateral panel. The value of corresponding integral depends only on the coordinates of each side and therefore the contribution from each side can be evaluated independently. In the free surface Green function model, the body surface is approximated by flat panels and the Rankine source and its image part can be analytically evaluated by this Hess-Smith method together with free surface boundary condition satisfied by a singular wave integral (Beck, 1994).

In the Rankine source approach the Rankine source does not

* Corresponding author.
E-mail address: a.feng@nus.edu.sg (A. Feng).
Peer review under responsibility of Society of Naval Architects of Korea.

https://doi.org/10.1016/j.ijnaoe.2018.02.001

satisfy the free surface boundary condition automatically and therefore the integral of Rankine source on free surface is required to evaluate. Cao et al. (1991); Lee (1992); Zhang et al. (2010); Wang et al. (2015) placed isolated control (collocation) points to represent the continuous free surface profile. By this treatment the integration of Rankine source over free surface panels is approximately calculated by the value of $1/r$ multiplying the corresponding panel surface area. In this method when the source point and control point are located in the same panel, the distance r becomes 0 and $1/r$ tends to ∞. In order to eliminate this singularity, they developed a desingularized technique by placing the isolated source points above the control points and therefore in their model these two kinds of points never coincide with each other. By this means the troublesome singularity is essentially removed. This treatment does simplify the numerical algorithm but numerical technique is required to deal with desingularized distance between source point and control point (Cao et al., 1991; Cao and Beck, 2016).

In this paper the Rankine source integrals on both body surface and free surface panels are calculated by the analytical expression of Hess-Smith method. To facilitate this, continuous panels on free surface need to be applied to discretise free surface profile. The integral of $1/r$ on the panel is integrable when the Rankine source points and control points are located in the same panel. The value of this integral can be obtained by a mathematical derivation (Chen, 2014). No desingularized technique is required to avoid singularity. As numerical errors arising from the boundary integral are eliminated this proposed method aims to improve the numerical accuracy and efficiency for various water wave problems.

The far field radiation condition requires careful treatment in the Rankine source model. The infinite free surface integral domain in this method is truncated to a bounded domain but the truncated boundary may cause a reflective wave propagation disturbance. Several numerical techniques are available to reduce non-physical wave reflection from the truncated boundary, amongst which a numerical beach is widely employed. This method was originated by Israeli and Orszag (1981) who added a Newtonian cooling term and a Reynolds viscosity damping term to the free surface boundary conditions. The former term acts as a damper absorbing free surface disturbances whereas the latter modifies the wave dispersion caused by this artificial damping. This method has been further extended to various wave-body problems and it is applicable to a large range oscillatory wave frequencies (Sclavounos and Nakos, 1988; Kring and Sclavounos, 1995; Kim et al., 1997). For example, to avoid wave reflection, Kim et al. (1997) employed a kinematic free surface condition equipped with Newtonian cooling and Rayleigh viscosity damping terms, whereas Tanizawa (1996); Koo and Kim (2004, 2007) added Newtonian cooling to the kinematic free surface boundary condition and introduced damping terms to the dynamic free surface boundary condition. However, the terms added to the free surface boundary conditions give rise to artificially induced numerical errors.

In the desingularized method developed by Lee (1992); Cao et al. (1993); Zhang and Beck (2008); Bandyk and Beck (2011), they divided the free surface range into inner and outer domains. The Rankine source points are placed in an exponentially increasing form in the outer domain and it covers a very large area of free surface range. Due to the periodic characteristics of progressive wave, the numerical computation is completed before the surface wave reaches the truncated boundary. This produces a postponement of the wave refection from the truncation boundary and satisfactory results can be obtained. This simple method is very efficient and free of artificial errors. In this paper this treatment is introduced into our proposed method to satisfy the far field radiation condition.

The source points distribution on the free surface is vital for the accuracy and efficiency of the boundary integral method. Recently Feng et al. (2015) applied a source point distribution method with increasing spaces between source points to replace the even space method for two dimensional water wave problems. This method places a higher density of source points near the floating body and, at distant from the body, a distribution of lesser density. Through this method, the number of source points is reduced and therefore the computational effort is significantly reduced with numerical accuracy retained or increased. This new source distribution method is further developed to accommodate this improved Rankine source method for three dimensional problems.

The novelty of the present study is twofold. First, analytical calculations for Rankine source integral are applied for both free surface and body surface rather than numerical approximate for isolated source points. Other researchers used either isolated source points or partial continuous panels to discretize the fluid surfaces as summarized in Table 1. Second, an uneven free surface source panel distribution scheme is developed to reduce computational cost whereas keep or increase numerical accuracy, as the application of analytical integral creating this possibility.

In this study, linear boundary condition is assumed and a third order Adams-Bashforth scheme is adopted in the free surface time stepping process. Following the background statement and literature review in Section 1, the boundary integral problem and mathematical formulation are demonstrated in Section 2 followed by numerical algorithm in Section 3. In Section 4 the numerical convergency of the proposed will be tested in Subsection 4.1. The validation and comparison will be presented for wave radiation problem in Subsection 4.2. In Subsection 4.3 numerical results for wave diffraction problem will be provided to further demonstrate the high accuracy and efficiency of the proposed method. Wave and current coexist problem is studied in Subsection 4.4 to show a broader application of the proposed method.

2. Problem formulation

2.1. Fluid motion equations

A coordinate frame of reference $OXYZ$ is defined with origin O at the centre of a three dimensional body floating in a fluid domain. The fluid domain Ω is bounded by a free surface S_f, body surface S_b, seabed surface S_0 and enclosing surface at infinity, S_∞. Fig. 1 shows the sketch of a three dimensional wave-body interaction problem.

The fluid flow is assumed irrotational and total velocity potential ϕ is subject to Laplace equation

$$\frac{\partial^2\phi}{\partial x^2}+\frac{\partial^2\phi}{\partial y^2}+\frac{\partial^2\phi}{\partial z^2}=0 \text{ in the fluid domain } \Omega \tag{1}$$

and can be described by

$$\phi(x,y,z,t)=Ux+\phi_u(x,y,z,t) \tag{2}$$

where U denotes steady uniform current and ϕ_u indicates unsteady velocity potential. The total velocity potential $\phi(x,y,z,t)$ is subject to physical boundary conditions on the body surface S_b, on free surface S_f and on the seabed S_0. These boundary conditions are expressed respectively as:

Table 1
Summary of numerical method for Rankine source integral and free surface source distribution method applied in earlier investigation.

Author(s)/(year)	Body surface	Free surface	Source dis.
Beck and King (1989)	Analyt.	Approx.	Even
Beck (1994)	Analyt.	Approx.	Even
Cao et al. (1990, 1991, 1993)	Approx.	Approx.	Even
Isaacson and Cheung (1991), Isaacson et al. (1993)	Approx.	Approx.	Even
Lee (1992, 2003)	Analyt.	Approx.	Even
Koo and Kim (2004, 2006, 2007)	Approx.	Approx.	Even
Zhang et al. (2006)	Approx.	Approx.	Even
Bandyk, 2009, Bandyk and Beck, 2011	Analyt.	Approx.	Even
Zhang and Beck (2007, 2008), Zhang et al. (2010)	Analyt.	Approx.	Even
Bai and Teng (2013)	Approx.	Approx.	Even
Wang et al. (2015, 2016)	Approx.	Approx.	Even

"Analyt." stands for analytical calculation for Rankine source integral.
"Approx." stands for approximation calculation for Rankine source integral.
"Even" stands for free surface even source panel distribution.

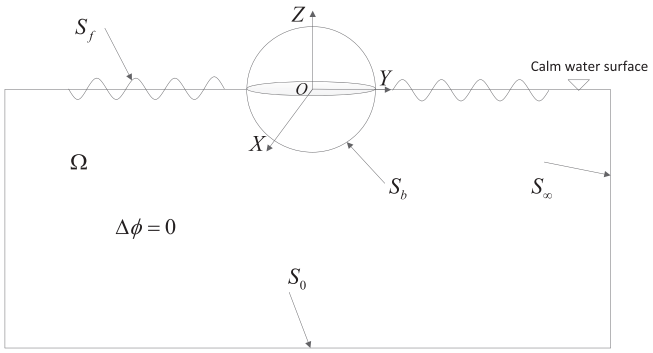

Fig. 1. Sketch of a three dimensional wave-body interaction problem.

$$\frac{\partial \phi}{\partial \mathbf{n}_b} = V_{n_b} \text{ on } S_b, \tag{3}$$

$$\frac{\partial \phi}{\partial z} - \frac{\partial \eta}{\partial t} = 0 \text{ on } S_f, \tag{4}$$

$$\frac{\partial \phi}{\partial t} + g\eta = 0 \text{ on } S_f, \tag{5}$$

$$\frac{\partial \phi}{\partial z} = 0 \text{ on } S_0. \tag{6}$$

Here $\mathbf{n}_b$ denotes the normal vector of the body surface pointing into the fluid domain. V_{n_b} denotes the local body surface velocity in the direction $\mathbf{n}_b$. η and g are free surface elevation and gravitational acceleration respectively.

By linear superposition, the unsteady velocity potential $\phi_u(x,y,z,t)$ can be further separated as:

$$\phi_u(x,y,z,t) = \phi_I(x,y,z,t) + \phi_D(x,y,z,t) + \phi_R(x,y,z,t), \tag{7}$$

where $\varphi_I(x,y,z,t)$ stands for the incident wave potential, $\phi_D(x,y,z,t)$ denotes the diffraction potential and ϕ_R indicates the radiation potential. For the incoming linear plane progressive wave in deep water condition, ϕ_I can be formulated as

$$\phi_I = \frac{gA}{\omega} e^{kz} \sin(kx - \omega t), \tag{8}$$

where g, A, ω and k are the gravitational acceleration, wave amplitude, wave frequency and wave number respectively.

Lamb (1945) expressed the velocity potential ϕ as a boundary integral of Rankine sources continuously distributed on the fluid boundary $S = S_b \cup S_f$ in the form

$$\phi(\mathbf{x}',t) = \int_{S_b} \sigma^b \frac{1}{|\mathbf{x}' - \mathbf{x}|} ds_{\mathbf{x}} + \int_{S_f} \sigma^f \frac{1}{|\mathbf{x}' - \mathbf{x}|} ds_{\mathbf{x}} + \int_{S_0} \sigma^0 \frac{1}{|\mathbf{x}' - \mathbf{x}|} ds_{\mathbf{x}}. \tag{9}$$

Here we denote control point $\mathbf{x}' = (x',y',z')$, source point $\mathbf{x} = (x, y,z)$, body source strength $\sigma^b = \sigma(x,t)$, free surface source strength $\sigma^f = \sigma(x,t)$ and seabed source strength $\sigma^0 = \sigma(x,t)$. In present, only deep water condition is considered and therefor the last integral on the right side of Eq. (9) disappears in the following part of this paper.

2.2. Numerical simulation process

In present simulation, the fluid domain surface S is discretized by panel Rankine sources rather than isolated Rankine source points. These panel sources are located exactly on the fluid domain surface S and therefore no desingularized distance is applied. Let the integral surfaces S_b and S_f be approximated as sums of panels N_b and N_f respectively such as $S_b = \cup_{i=1}^{N_b} S_i^b$ and $S_f = \cup_{j=1}^{N_f} S_j^f$.

Therefore, the discretization of Eq. (9) is given by

$$\phi(\mathbf{x}',t) = \sum_{i=1}^{N^b} \sigma_i^b \int_{S_i^b} \frac{1}{|\mathbf{x}' - \mathbf{x}_i|} ds_{\mathbf{x}} + \sum_{j=1}^{N^f} \sigma_j^f \int_{S_j^f} \frac{1}{|\mathbf{x}' - \mathbf{x}_j|} ds_{\mathbf{x}}. \tag{10}$$

Let $\mathbf{x}_i^b \in S_b$, $\mathbf{x}'^b_i \in S_b$ and $\mathbf{x}_j^f \in S_f$, $\mathbf{x}'^f_j \in S_f$ be source points and control points respectively for $i = 1, \ldots, N^b$ and $j = 1, \ldots, N^f$. These control points are located at the centre of three dimensional surface panels. With the use of the body boundary conditions (3) and the boundary integral Eq. (10) with its normal derivative, we solve the source strengths σ_i^b and σ_j^f on S_i^b and S_j^f from the following equations

$$\phi\left(\mathbf{x}'^f_j, t\right) = \sum_{i=1}^{N^b} \sigma_i^b \int_{S_i^b} \frac{1}{\left|\mathbf{x}'^f_j - \mathbf{x}_i^b\right|} ds_{\mathbf{x}} + \sum_{j=1}^{N^f} \sigma_j^f \int_{S_j^f} \frac{1}{\left|\mathbf{x}'^f_j - \mathbf{x}_j^f\right|} ds_{\mathbf{x}}, \tag{11}$$

$$V_{n_b}\left(\mathbf{x}'^b_i,t\right)=\sum_{i=1}^{N^b}\sigma_i^b\frac{\partial}{\partial n_b^i}\int\limits_{S_i^b}\frac{1}{\left|\mathbf{x}'^b_i-\mathbf{x}_i^b\right|}ds_{\mathbf{x}}+\sum_{j=1}^{N^f}\sigma_j^f\frac{\partial}{\partial n_b^i}\int\limits_{S_j^f}\frac{1}{\left|\mathbf{x}'^b_i-\mathbf{x}_j^f\right|}ds_{\mathbf{x}}. \tag{12}$$

Here V_{n_b} represents the normal velocity on the panels of the body surface S_i^b, and $\mathbf{n}_b^i$ denotes the unit normal vector on the panel S_i^b.

Eqs. (11) and (12) can be formulated in the following matrix format:

$$\begin{bmatrix}A_{N_fN_b} & A_{N_fN_f}\\ A_{N_bN_b} & A_{N_bN_f}\end{bmatrix}\begin{bmatrix}\sigma^b\\ \sigma^f\end{bmatrix}=\begin{bmatrix}\phi\left(\mathbf{x}'^f_j,t\right)\\ V_{n_b}\end{bmatrix}, \tag{13}$$

where $[A_{mn}](m=N_f,N_b$ and $n=N_f,N_b)$ are influence coefficient blocks. They reflect the influence of a source panel n on the control point of panel m. The evaluation of $A_{N_fN_b}$ and $A_{N_fN_f}$ requires the integral of Rankine source $1/r$ on the three dimensional panel. The calculation for $A_{N_bN_b}$ and $A_{N_bN_f}$ involve with the derivative of the integral of Rankine source $1/r$ on the three dimensional panel. The first two influence coefficient blocks can be calculated in the same method while the last two are evaluated in the same way. The calculation of these influence coefficients involves transformation of three dimensional element panel in global coordinate system into quadrilateral element in local element coordinate system first and inverse transformation back to global coordinate system. Fig. 2 shows the three dimensional numerical model sketch.

The substitution of the source strength values σ_i^b and σ_j^f at time t obtained from the set of Eqs. (11) and (12) produces calculation of the normal velocity $v_{fz}(\mathbf{x}'^f_j,t)=\frac{\partial\phi(\mathbf{x}'^f_j,t)}{\partial z}$ on the free surface as

$$v_{fz}\left(\mathbf{x}'^f_j,t\right)=\sum_{i=1}^{N^b}\sigma_i^b\frac{\partial}{\partial z}\int\limits_{S_j^b}\frac{1}{\left|\mathbf{x}'^f_j-\mathbf{x}_i^b\right|}ds_{\mathbf{x}}+\sum_{j=1}^{N^f}\sigma_j^f\frac{\partial}{\partial z}\int\limits_{S_j^b}\frac{1}{\left|\mathbf{x}'^f_j-\mathbf{x}_j^f\right|}ds_{\mathbf{x}}. \tag{14}$$

In this paper, the free surface source point $\mathbf{x}'^f_j$ and control point $\mathbf{x}_j^f$ coincide with each other on every free surface panel. The second term on the right side of Eq. (14) can be regarded as the velocity in the z direction induced by a source located on the free surface. When the source point $\mathbf{x}'^f_j$ and control point $\mathbf{x}_j^f$ are in the same panel, this item is corresponding to the velocity induced on the source panel surface, therefore we have (Chen, 2014),

$$\frac{\partial}{\partial z}\int\limits_{S_j^f}\frac{1}{\left|\mathbf{x}'^f_j-\mathbf{x}_j^f\right|}=2\pi.$$

When the source point $\mathbf{x}_j^f$ and control point $\mathbf{x}_j^f$ are not in the same panel, because they are located in the same horizontal line on the calm water surface, the source panel provides no contribution on the fluid velocity in the z direction, so we have

$$\frac{\partial}{\partial z}\int\limits_{S_j^f}\frac{1}{\left|\mathbf{x}'^f_j-\mathbf{x}_j^f\right|}=0.$$

The matrix format for this item can be formulated as:

$$\sum_{j=1}^{N^f}\frac{\partial}{\partial z}\int\limits_{S_j^f}\frac{1}{\left|\mathbf{x}'^f_j-\mathbf{x}_j^f\right|}=\begin{bmatrix}2\pi & 0 & \cdots & 0\\ 0 & 2\pi & \cdots & 0\\ \vdots & \vdots & \ddots & \vdots\\ 0 & 0 & \cdots & 2\pi\end{bmatrix}. \tag{15}$$

For the traditional isolated source point method, Eq. (9) is discretized as:

$$\phi(\mathbf{x}',t)=\sum_{i=1}^{N^b}\sigma_i^b\frac{1}{|\mathbf{x}'-\mathbf{x}_i|}ds_{\mathbf{x}}+\sum_{j=1}^{N^f}\sigma_j^f\frac{1}{|\mathbf{x}'-\mathbf{x}_j|}ds_{\mathbf{x}}. \tag{16}$$

Following this discretization method, Eqs. (11) and (12) are expressed as:

$$\phi\left(\mathbf{x}'^f_j,t\right)=\sum_{i=1}^{N^b}\sigma_i^b\frac{1}{\left|\mathbf{x}'^f_j-\mathbf{x}_i^b\right|}ds_{\mathbf{x}}+\sum_{j=1}^{N^f}\sigma_j^f\frac{1}{\left|\mathbf{x}'^f_j-\mathbf{x}_j^f\right|}ds_{\mathbf{x}}, \tag{17}$$

$$V_{n_b}\left(\mathbf{x}'^b_i,t\right)=\sum_{i=1}^{N^b}\sigma_i^b\frac{\partial}{\partial n_b^i}\frac{1}{\left|\mathbf{x}'^b_i-\mathbf{x}_i^b\right|}ds_{\mathbf{x}}+\sum_{j=1}^{N^f}\sigma_j^f\frac{\partial}{\partial n_b^i}\frac{1}{\left|\mathbf{x}'^b_i-\mathbf{x}_j^f\right|}ds_{\mathbf{x}}. \tag{18}$$

It should be noticed that the source point and control point can

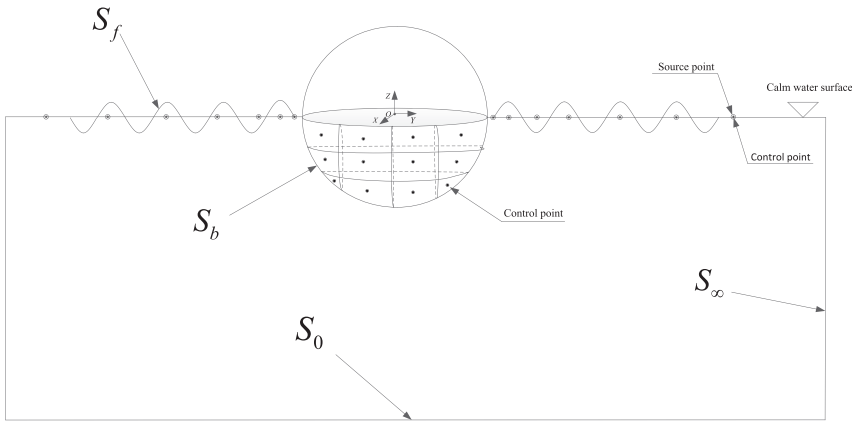

Fig. 2. Three dimensional numerical model sketch.

never be coincide with each other and desingurized method has to be adopted to keep these two kinds of points in a reasonable distance.

2.3. Free surface time-stepping scheme

The free surface conditions are updated according to Eqs. (4) and (5) by a 3rd-order Adams-Bashforth scheme. At initial time $t = 0$, the free surface is assumed still and therefore we have $\phi(\mathbf{x}'^f_j, 0) = 0$ for every control panel in the free surface. Then source strength σ_b and σ_f can be obtained by solving Eq. (13). After that $v_{fz}(\mathbf{x}'^f_j, 0)$ is evaluated by Eq. (14). Then free surface time-stepping scheme is started to get the information for $\phi(\mathbf{x}'^f_j, \Delta t)$ for the next time step simulation. Starting from $t = 0$, the free surface time-stepping can be expressed as:

$$\eta(\Delta t) = v_{fz}(0)\Delta t, \tag{19}$$

$$\phi(\Delta t) = -g\eta(\Delta t)\Delta t, \neq \tag{20}$$

and in a 2nd-order Adam-Bashforth scheme, we have

$$\eta(2\Delta t) = \eta(\Delta t) + \frac{\Delta t}{2}\Big[3(v_{fz}(\Delta t) - v_{fz}(0)\Big], \tag{21}$$

$$\phi(2\Delta t) = \phi(\Delta t) + \frac{\Delta t}{2}[-3g\eta(\Delta t) + g\eta(0)], \frac{\delta y}{\delta x} \tag{22}$$

When the 3rd-order Adam-Bashforth scheme is adopted, we have

$$\eta(t + \Delta t) = \eta(t) + \frac{\Delta t}{12}\Big[23v_{fz}(t) - 16v_{fz}(t - \Delta t) + 5v_{fz}(t - 2\Delta t)\Big], \tag{23}$$

$$\phi(t + \Delta t) = \phi(t) + \frac{\Delta t}{12}[-23g\eta(t) + 16g\eta(t - \Delta t) - 5g\eta(t - 2\Delta t)]. \tag{24}$$

With strengths σ^b_i and σ^f_j determined, the velocity potentials on the body surface S_b are derived from Eq. (9) in the form:

$$\phi\Big(\mathbf{x}'^b_i, t\Big) = \sum_{i=1}^{N^b}\sigma^b_j \int\limits_{S^b_i} \frac{1}{|\mathbf{x}'^b_i - \mathbf{x}^b_i|} ds_{\mathbf{x}} + \sum_{j=1}^{N^f}\sigma^f_j \int\limits_{S^f_j} \frac{1}{\left|\mathbf{x}'^b_i - \mathbf{x}^f_j\right|} ds_{\mathbf{x}}. \tag{25}$$

The evaluation of the two terms on the right side of Eq. (25) involves the integral of Rankine source on the three dimensional panel. The calculations for these terms are similar as A_{NfNf} and A_{NfNb}.

The hydrodynamic pressure on the body surface, $p(t) = p(\mathbf{x}'^b_i, t)$, is evaluated from Bernoulli equation expressed as

$$\frac{p(t)}{\rho} = -\frac{\partial\phi}{\partial t} \tag{26}$$

where ρ denotes the fluid density.

The dynamic force $F(t)$ applied to the body surface is calculated by integrating the dynamic pressure over the body surface as given by

$$F(t) = \int\limits_{S_b} p(t)n_b ds. \tag{27}$$

By Fourier transform, added mass $a_{kk}(\omega)$ ($k = 2$, for surge motion and $k = 3$ for heave motion) and damping coefficient $b_{kk}(\omega)$ can be obtained as:

$$a_{kk}(\omega) = \frac{2}{a\omega^2 T_0}\int\limits_0^{T_0} F_{kk}(t)\sin(\omega t)dt, \tag{28}$$

$$b_{kk}(\omega) = -\frac{2}{a\omega T_0}\int\limits_0^{T_0} F_{kk}(t)\cos(\omega t)dt, \tag{29}$$

where $F_{kk}(t)$,a, T_0 are the radiation force, body motion amplitude and motion period respectively. The non-dimensional added mass coefficient A_{kk} and damping coefficient B_{kk} can be formulated by body volume ∇, fluid density ρ in the format of

$$A_{kk} = \frac{a_{kk}}{\rho\nabla}, \tag{30}$$

$$B_{kk} = \frac{b_{kk}}{\rho\omega\nabla}. \tag{31}$$

The integrals in Eqs. (28) and (29) are numerically calculated by the sum of $F_{kk}(t)sin(\omega t)\Delta t$ or $F_{kk}(t)cos(\omega t)\Delta t$. Here Δt is the time step, which is same as that applied in the time stepping process. In present study, the force responses become very stable after two periods. Therefore, the integral is calculated starting from the third period and ending after fourth period. The average value of these two periods is chosen as the value for the integral. By this means, the numerical error to evaluate the integral can be minimized. However, it should be noticed that this method is only applicable for smaller oscillatory frequency ω. The values of summations of $F_{kk}(t)sin(\omega t)\Delta t$ or $F_{kk}(t)cos(\omega t)\Delta t$ become highly oscillatory when frequency ω becomes higher than a certain value. In this case, the selection of Δt should be given careful consideration.

3. Numerical implementation

In the application of the proposed numerical methods to simulate wave radiation and diffraction problems, a number of numerical techniques closely related to the numerical performance have to be applied. These numerical techniques have a direct effect on the numerical accuracy and efficiency and are discussed in this section.

3.1. Fluid domain panel distribution

The fluid domain surface is composed of a body surface S_b and free surface S_f. Body surface S_b and free surface S_f are approximated by quadrilateral panels instead of isolated source points. These panels coincide with their respective surface profiles and the source point on each panel is located at the same position as control point. Fig. 3 shows the profile of Rankine source panel distribution on free surface.

Free surface source points are kept still in the global coordinate system in the time stepping process for linear wave problems. Polar coordinate system is applied to facilitate the free surface source point distribution. In the radial direction the free surface is divided into inner and outer domains. The accuracy and efficiency of the

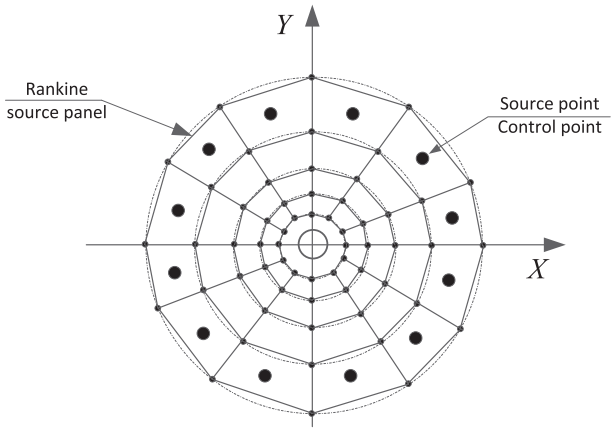

Fig. 3. Profile of Rankine source panel distribution on free surface.

numerical simulation largely depend on the panel distribution. To approximate the free surface in the inner domain, the horizontal distances between the center of neighbouring free surface source panels are expressed in the form:

$$\left|\mathbf{x}_j'^f - \mathbf{x}_{j-1}'^f\right| = \frac{L_b\alpha_j}{\omega^2} \quad \text{in the inner domain} \tag{32}$$

$$\left|\mathbf{x}_j'^f - \mathbf{x}_{j-1}'^f\right| = \frac{L_b\alpha_j}{\omega^2}1.05^{j(j-1)/2} \quad \text{in the outer domain,} \tag{33}$$

where L_b is the area of the body surface panel covering the intersection point of the body and free surface. The parameters α_j define the separation distances and are decided according to the method discussed by Feng et al. (2015) which for this reason, is omitted herein. As shown in Eq. (33), the distances of the center of neighbouring source panel are displaced in an exponentially increasing form. By this means very large area of free surface is covered and therefore the generated wave can move towards the infinity without wave reflection caused by the truncated boundary. In this method there are 40 source panels in the inner domain and 10 panels in the outer domain in the radial direction.

As only linear wave problem is investigated in present study, it should be noticed that computational domain and the boundaries of S_b, S_f and S_o remain unchanged during the whole time-domain solution procedure. The free surface S_f is essentially a flat horizontal plane, thus the source panels on the free surface are flat panels.

3.2. Algebraic equation solver

The present formulation needs to solve the matrix Eq. (13) to obtain source strength and then calculate the velocity potential ϕ_b on the body surface S_b and normal velocity V_{fz} on the free surface S_f. This algorithm is named as "indirect method" according to the definition of Cao et al. (1993). Compared to the so called "direct method", this algorithm can give an insight of the source strength and accordingly guide the Rankine source panel distribution.

Additionally this method doesn't require re-assembling the influence matrix $[A_{mn}]$ at every time step. Once the influence matrix is established at initial time, it can be used over the whole simulation and therefore the computational cost is reduced. In present simulation, the influence matrix $[A_{mn}]$ together with the inverse influence matrix $[A_{mn}]^{-1}$ is evaluated at initial time $t = 0$. The source strength σ^f and σ^b are calculated by multiplying $[A_{mn}]^{-1}$ with the right side of Eq. (13) at every time step.

3.3. Ramp function

During the initial time steps, an abrupt initial condition should be avoided. A cosine ramp function F_m is applied here to modulate the body surface condition. F_m is formulated as:

$$F_m = \begin{cases} \frac{1}{2}\left[1 - cos\left(\frac{\pi t}{T_0}\right)\right] & t < T_m \\ 1 & t \geq T_m \end{cases} \tag{34}$$

where T_m is a ramp time and it is here uniformly chosen as one excitation period T_0 for both wave radiation and diffraction problems.

4. Numerical results

Numerical results for linear wave radiation and diffraction problems are presented to show the high accuracy and efficiency of the proposed method in this section. These two problems are investigated separately and therefore no coupling effects are considered. The numerical simulation is executed in time domain and the results are transformed into frequency domain for the purpose of comparison. All the yielding results are presented in non-dimensional form and the method to nondimensionlize these data will be explained where necessary.

4.1. Numerical convergency

The radiation problem induced by a hemisphere is investigated to demonstrate the numerical convergency of the proposed method. At initial time the hemisphere is about to start oscillatory motion from its equilibrium position and fluid is still everywhere in the whole fluid domain. The hemisphere surface is formulated by a spherical coordinate system

$$\begin{aligned} x &= R\cos\theta\sin\varphi(0 \leq \theta \leq 2\pi, 0 \leq \varphi \leq \pi), \\ y &= R\sin\theta\sin\varphi(0 \leq \theta \leq 2\pi, 0 \leq \varphi \leq \pi), \\ z &= R\cos\varphi\left(0 \leq \varphi \leq \frac{\pi}{2}\right). \end{aligned} \tag{35}$$

Here R denotes the radius of the hemisphere. θ and φ are polar and azimuth angles respectively. The wetted hemisphere surface is divided evenly with 20 sections in θ and 20 sections in φ in both latitude and longitude directions.

In order to demonstrate the accuracy of the proposed method, an error coefficient C_e is introduced to exam the agreement between predicted hydrodynamic coefficients and analytical linear results of Hulme (1982). C_e is defined as

$$C_e = \frac{\sqrt{\left((A_{33} - A'_{33})/A'_{33}\right)^2 + \left((B_{33} - B'_{33})/B'_{33}\right)^2}}{2}, \tag{36}$$

where A_{33}, B_{33} and A'_{33}, B'_{33} are added mass coefficients and damping coefficients obtained respectively from the numerical prediction and the analytical formulation of Hulme (1982).

As mentioned in the last section, in the radial direction 55 points are required to cover both inner and outer domains on the free surface. In order to test the numerical accuracy, the free surface is divided into 4, 6, 8, 9, 10 portions respectively in the axial direction. Table 2 shows the error coefficient C_e with different portion numbers at three kR numbers. The value of error coefficients tends to a very small steady value when portion number is 10 and the

Table 2
Error coefficient C_e between the analytical results of Hulme (1982) and the proposed method respect to different portion number on free surface.

Portion no.	*kR*		
	0.8	1.0	1.2
4	3.03%	2.39%	2.37%
6	1.42%	0.91%	1.61%
8	0.93%	0.84%	1.37%
9	0.61%	0.44%	0.32%
10	0.49%	0.41%	0.28%

decreasing rate becomes very low beyond 10. Therefore portion number 10 in the axial direction is selected in the following numerical simulation. In summary there are 400 panels on body surface and 500 panels on free surface in present simulation. It is noticed that similar numbers of panels are required to cover the body surface and free surface. This is reasonable because the body surface is a curved surface while calm free surface is a flat surface. More flat quadrilateral panels are required to discretize the curve surface than the flat surface based on the principle of Hess-smith method.

4.2. Wave radiation by a hemisphere and truncated circular cylinder experiencing forced oscillatory motions

The radiation problem induced by a sphere and a truncated vertical circular cylinder is further investigated to demonstrate the accuracy and efficiency of the proposed method. Table 3 show comparisons of error coefficient C_e between proposed method results and numerical results of Zhang and Beck (2008). All the value of C_e in our proposed method is below 1% and the proposed method shows a largely reduction of the value of C_e compared with the data of Zhang and Beck (2008).

In order to demonstrate a broader range of comparison between proposed method results and available data in literature. Figs. 4 and 5 show predicted heave added mass coefficient A_{33} and damping coefficient B_{33} evaluated by the proposed method compared with the analytical data of Hulme (1982) and numerical results of Zhang and Beck (2008) adopting an isolated source point module on free surface discretization. As expected the proposed method shows a closer agreement with the analytical results of Hulme (1982) across the frequency range and this is especially true for the damping coefficient B_{33} when the oscillatory frequency kR is greater than 1.0.

Figs. 6 and 7 demonstrate comparison of the time record of heave force $F_{33}(t)$ and surge force $F_{11}(t)$ between proposed method results and Hulme (1982) analytical results for the sphere experiencing oscillatory heave and surge motion respectively with motion frequency $kR = 1.0$. It is observed that the proposed method shows a favorable agreement with the analytical results in time domain. In this section the produced force F_{33} and F_{11} in both frequency domain and time domain are nondimensionalized in the same way as $F_{33} = F_{33}/\rho g\pi R^2 a$ and $F_{11} = F_{11}/\rho g\pi R^2 a$.

Numerical simulation is further applied to a truncated circular

Table 3
Comparisons of error coefficient C_e between proposed method results and numerical results of Zhang and Beck (2008).

kR	Zhang and Beck (2008)	Proposed method
0.4	2.65%	0.90%
0.8	0.91%	0.49%
1.2	2.19%	0.28%
1.6	2.44%	0.61%
2.0	2.96%	0.12%

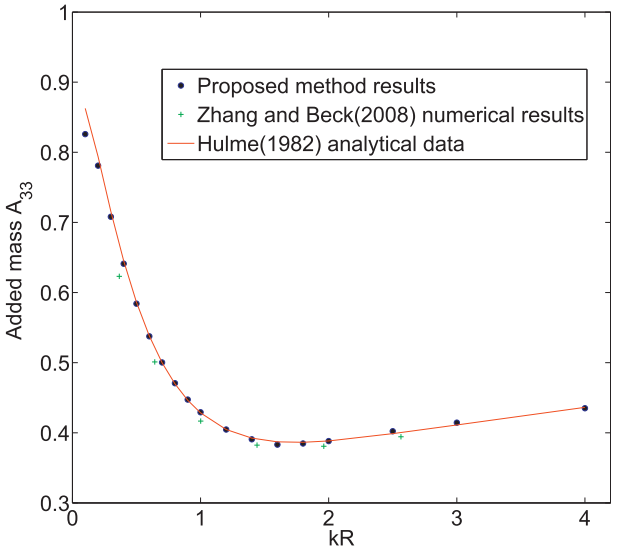

Fig. 4. Comparison of heave added mass coefficient A_{33} between proposed method results, isolated source point method results of Zhang and Beck (2008) and Hulme (1982) analytical results for a sphere experiencing oscillatory heave motion.

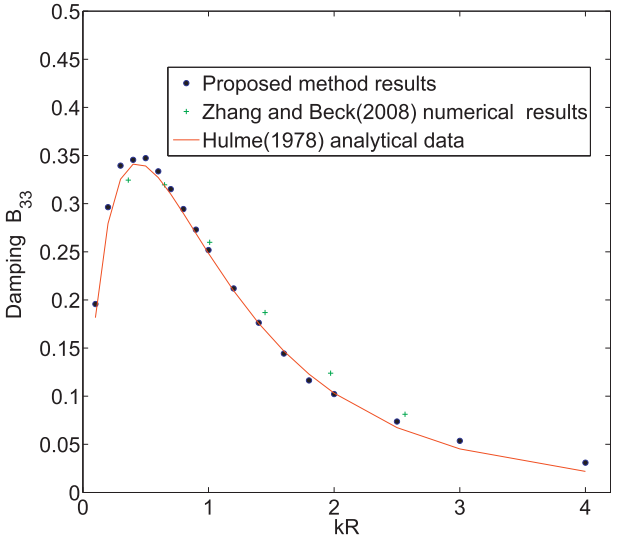

Fig. 5. Comparison of heave damping coefficient B_{33} between proposed method results, isolated source point method results of Zhang and Beck (2008) and Hulme (1982) analytical results for a sphere experiencing oscillatory heave motion.

cylinder with radius R and draft $B = 0.5R$. Fig. 8 show the comparison of heave force $F_{33}(\omega)$ (a) and surge force $F_{11}(\omega)$ (b) between the proposed method results and numerical prediction of Isaacson et al. (1993) who applied a high order Gaussian numerical integration. It is observed that the force amplitudes show a good agreement with the published data for both heave and surge motions in frequency domain.

The computational effort associated with the evaluations of matrix coefficients and the matrix inversion are proportional to N^2 and N^3 respectively, where N is the rank of the matrix coefficients. For the numerical method of Isaacson et al. (1993), about $3600 - 4800$ quadrilateral facets are typically generated to present whole boundary. For the isolated source point distribution method developed by Zhang and Beck (2008), 2340 source points are distributed to cover a hemisphere body surface and free surface. It's

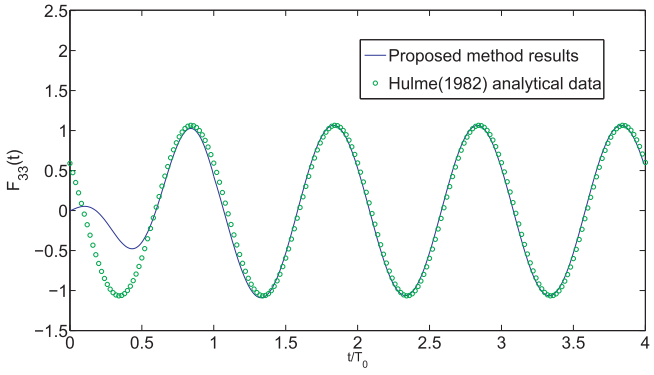

Fig. 6. Comparison of time record of heave force $F_{33}(t)$ between proposed method results and Hulme (1982) analytical results for a sphere experiencing oscillatory heave motion with motion frequency $kR = 1.0$.

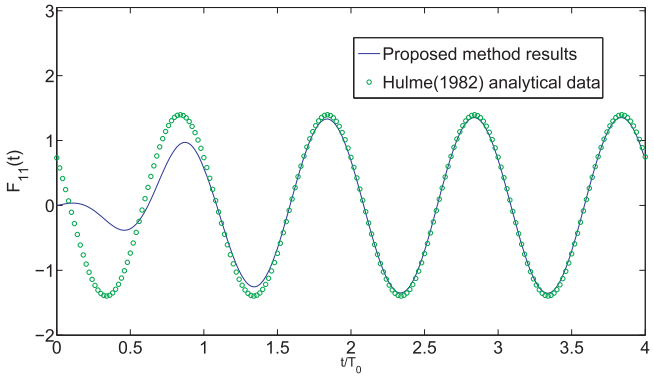

Fig. 7. Comparison of time record of surge force $F_{11}(t)$ between proposed method results and Hulme (1982) analytical results for a sphere experiencing oscillatory surge motion with motion frequency $kR = 1.0$.

expected that similar number of panels is required to cover a circular cylinder and the free surface though it is impossible to get a detailed information in the literature.

For the simulation of a circular cylinder in this paper, 400 panels are required to represent the body surface and 1000 panels are applied to cover the free surface. Recall that totally 900 panels are required to cover the whole fluid boundary for a hemisphere in the last section. Therefore it is reasonably summarized that about $900 - 1400$ quadrilateral panels are required to cover the whole boundary domain for a regular body in the proposed method.

Table 4
Comparisons of panel numbers between numerical methods of Isaacson et al. (1993), Zhang and Beck (2008) and proposed method.

Panel number		
Isaacson et al. (1993)	Zhang and Beck (2008)	Proposed method
$3600 - 4800$	2340	900–1400

A collection of the panel numbers applied in these three different methods are presented in Table 4 for a direct comparison. The proposed method only requires one third of panel number applied in the method of Isaacson et al. (1993). Compared with the method of Zhang and Beck (2008), the reduction of panel numbers seems less significant than that of Isaacson et al. (1993) and about one half of panel numbers are required in our method. However our method has shown a higher accuracy than the numerical model of Zhang and Beck (2008) in Table 2. For the same level of accuracy, the proposed method only requires about $600(= 400 + 4 \times 50)$ to $700(= 400 + 6 \times 50)$ panels to cover the whole fluid domain. Less than one third of panel numbers are needed compared to their method. Apart from the exact calculation of Rankine source integral applied in our proposed method, the development of numerical scheme avoiding the application of desingularized technique is believed to also contribute the improvement.

Fig. 9 demonstrate the comparison of the time record of heave force $F_{33}(t)$ $(a)$and surge force $F_{11}(t)$ (b) respectively between proposed numerical method results and numerical prediction of Bai and Teng (2013) for a truncated circular cylinder experiencing oscillatory heave and surge motion with frequency $kR = 1.6$. Fig. 10 shows the comparison of the time record of wave elevation $\eta(t)$ between proposed numerical method results and the numerical prediction of Bai and Teng (2013) for a truncated circular cylinder experiencing heave (a) and surge (b) motion respectively with motion frequency $kR = 1.6$. Wave elevation $\eta(t)$ is non-dimensionalized as $\eta(t) = \eta(t)/a$. The wave elevation is examined at the third control point on the free surface. These time domain

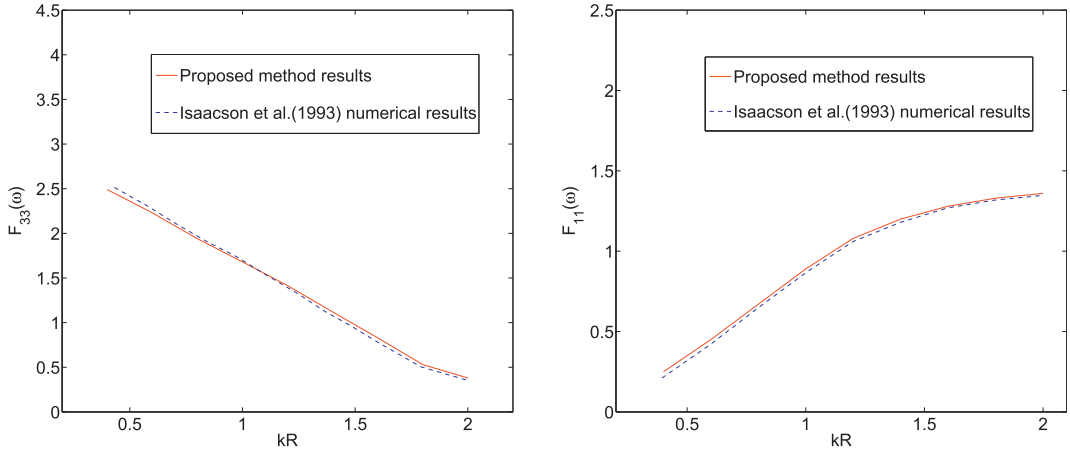

(a) Heave force $F_{33}(\omega)$ (b) Surge force $F_{11}(\omega)$

Fig. 8. Comparison of heave force $F_{33}(\omega)(a)$ and surge force $F_{11}(\omega)$ (b) between proposed method results and numerical prediction of Isaacson et al. (1993) for a truncated circular cylinder experiencing oscillatory heave and surge motion respectively.

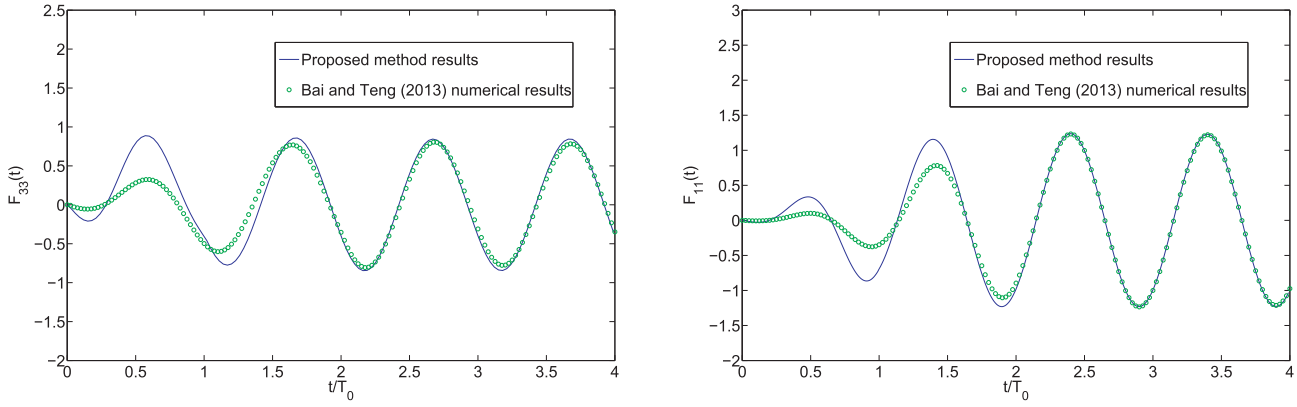

(a) Heave force $F_{33}(t)$ (b) Surge force $F_{11}(t)$

Fig. 9. Comparison of time record of oscillatory heave force $F_{33}(t)(a)$ and surge force $F_{11}(t)$ (b) between proposed method results and Bai and Teng (2013) numerical results for a truncated circular cylinder experiencing heave and surge motion with motion frequency $kR = 1.6$.

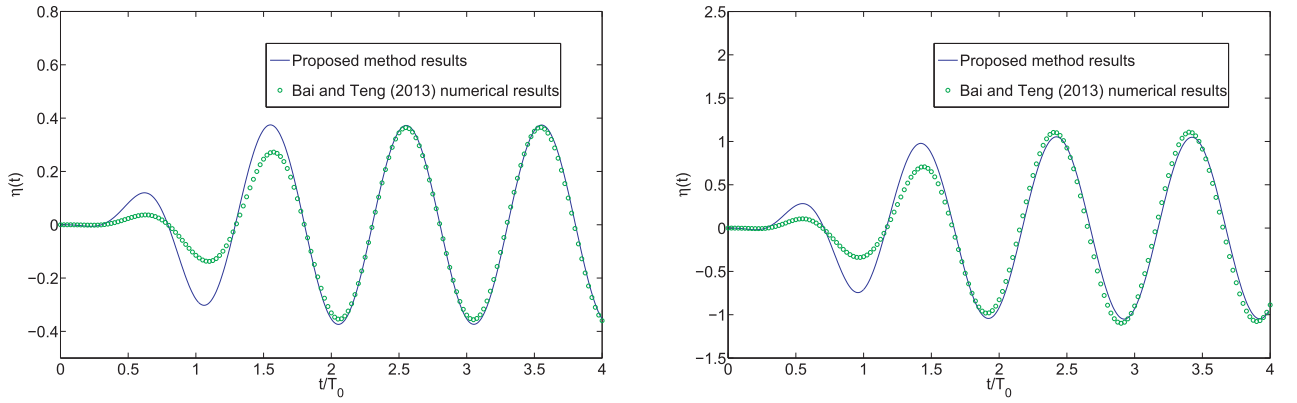

(a) Wave elevation $\eta(t)$ by heave motion (b) Wave elevation $\eta(t)$ by surge motion

Fig. 10. Comparison of wave elevation $\eta(t)$ between proposed method results and Bai and Teng (2013) numerical results for a truncated circular cylinder experiencing heave motion (a) and surge motion (b) with motion frequency $kR = 1.6$.

results show that a steady-state solution is developed after one wave period modulation time and agrees well with the numerical data of Bai and Teng (2013) in terms of amplitude and phase.

4.3. Wave diffraction around a hemisphere

In this section wave diffraction problem is investigated involving with a hemisphere fixed in the fluid domain. The radiation problem is excluded in the study because this floating body is still in the numerical simulation. The total diffraction force F is the sum of Froude-Krylov force and diffraction exciting force. The discretization of hemisphere surface is same as that for radiation problem.

Same as the method applied by Cao et al. (1991); Zhang and Beck (2008), a numerical code based on isolated source point is also developed to demonstrate the high accuracy and efficiency of the proposed method. For the proposed method, $600(50 \times 12)$ source panels are required to cover the whole free surface domain. For the isolated source point method, two different source panel numbers are applied: $1100(50 \times 22)$ and $1600(50 \times 32)$ panels are placed in the inner and outer domains. In summary, the proposed method needs $1000(600 + 400)$ panels to cover both body surface and free surface while the isolated source point methods require $1500(1100 + 400)$ and $2000(1600 + 400)$ sources respectively.

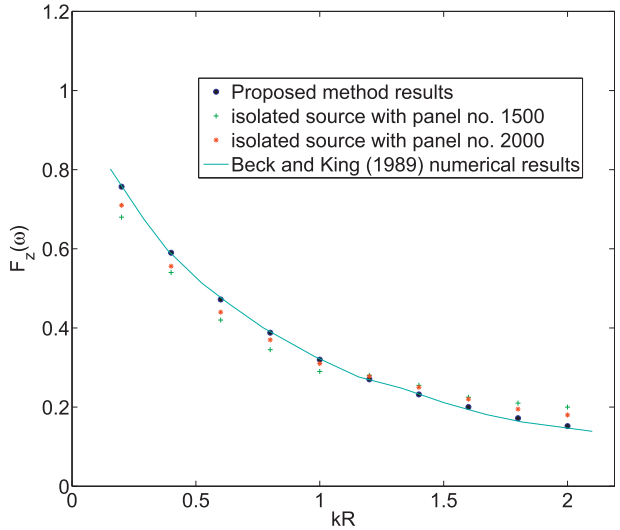

Fig. 11. Comparison of vertical total diffraction force $F_z(\omega)$ between proposed method results, isolated source point method with source point number 1500 and 2000 respectively, and numerical results of Beck and King (1989) for a hemisphere subject to a linear incident wave.

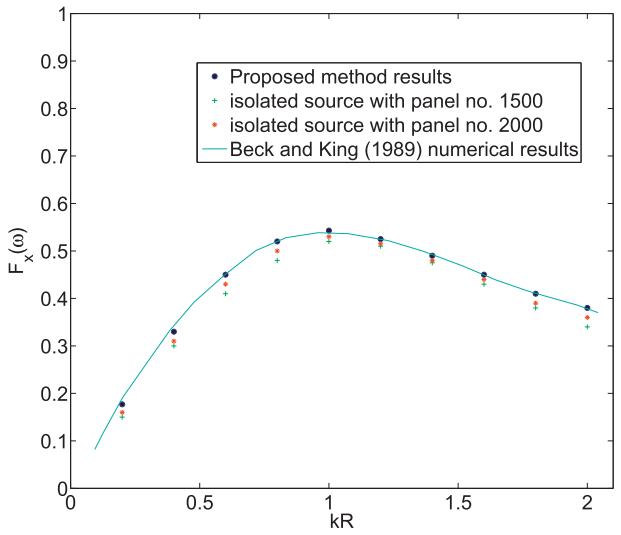

Fig. 12. Comparison of horizontal total diffraction force $F_x(\omega)$ between proposed method results, isolated source point method with source point number 1500 and 2000 respectively, and numerical results of Beck and King (1989) for a hemisphere subject to a linear incident wave.

Figs. 11 and 12 shows the comparison of vertical and horizontal total diffraction forces $F_z(\omega)$ and $F_x(\omega)$ respectively between proposed method results, numerical results of isolated source point model and numerical predictions of Beck and King (1989) utilizing a free surface Green function method. F_z and F_x are non-dimensionalized as $F_z(\omega) = F_z(\omega)/\rho g\pi R^2 a$ and $F_x(\omega) = F_x(\omega)/\rho g\pi R^2 a$. It is observed the proposed method results show an nearly perfect agreement with the numerical prediction of Beck and King (1989). The isolated source point method with the source point number 2000 has a closer agreement than this method with source point number 1500 but it is still less closer than the proposed method. Therefore the proposed method largely improves the numerical accuracy as well as numerical efficiency. In order to further demonstrate the efficiency of the proposed method, numerical simulations are carried out for $5T_0$ simulation for these two different methods. All the computations are carried out on a personal PC with CPU @2.6GHz and RAM 16 GB. Table 5 shows the panel numbers and computing time for these two methods. The proposed method only takes one half and one fourth computing time of the isolated source point method with panel numbers 1500 and 2000 respectively. The reduction of computing time for the proposed method further demonstrate the high accuracy and efficiency of the proposed method.

Fig. 13 demonstrate the comparison of time record of vertical total diffraction force $F_z(t)$ (a) and horizontal total diffraction force $F_x(t)$ (b) for this hemisphere subject to the linear incident wave with wave frequency $kR = 1.0$ between proposed method result and numerical prediction of Beck and King (1989). The time domain results of Beck and King (1989) are produced by Fourier transform from frequency domain results. These comparisons show perfect agreement between two numerical predictions in time domain.

Table 5
Comparisons of panel numbers and computing time between the isolated source point method and proposed method for $5T_0$ numerical simulation.

Method	Isolated source point method		Proposed method
Panel number	2000	1500	1000
Computing time (min.)	8	4	2

4.4. Wave diffraction around a hemisphere with current effect

In order to demonstrate a broader application of the proposed method, this continuous panel method is further developed to study wave diffraction problem considering current effect. Froude number Fr, which is designed to measure current speed, is defined as $Fr = U/\sqrt{(gR)}$. Current comes from the left and move towards positive x direction. Linear incoming wave and current act on a fixed hemisphere together.

Figs. 14 and 15 show the comparison of vertical force $F_z(\omega)$ and horizontal force $F_x(\omega)$ respectively between proposed method results and numerical prediction of Nossen et al. (1991) which applied free surface Green function method. These comparisons show the proposed method has a favourite agreement with numerical method of Nossen et al. (1991) for wave-current coexist problem.

5. Conclusions

An improved Rankine source panel method is developed to study three dimensional water wave problems. Both the free surface and body surface are discretized into continuous panels rather than traditional isolated source points. The surface integrals are calculated analytically instead of numerical approximation in tradition methods. As higher numerical accuracy obtained by this analytical calculation for Rankine source integral, the space increment source distribution method is therefore developed with the purpose to reduce computational cost while keep the numerical accuracy for water wave problems. Earlier investigations by numerical approximation or partially analytical calculation can produce high accuracy but they generally requires much more computational effort.

The free surface is divided into inner and outer domains. By distributing source point in an exponential form in outer domain, a very large area of free surface is covered and therefore the generated wave can move towards the infinity without wave reflection caused by the truncated boundary. By this simple and efficient numerical technique, the radiation boundary condition is well satisfied without artificial damping.

Numerical simulations are first performed for a hemisphere experiencing forced oscillatory motions. An error coefficient C_e comparing relative errors of added mass and damping coefficient is introduced to demonstrate the numerical accuracy. In the numerical convergency test the value of C_e for the proposed method shows less than 0.5% compared with analytical results when only 500 source panels are distributed to cover the whole free surface. By distributing this number of panels the proposed method produces much smaller C_e than the method of Zhang and Beck (2008) which applied numerical approximation to calculate the Rankine source integral. For the truncated cylinder case, the proposed method shows good agreement with the numerical results of Isaacson et al. (1993) which applies the high order numerical approximation. For these two cases, the proposed method requires about $900 - 1400$ source panels to cover the whole fluid domain while the methods of Zhang and Beck (2008) and Isaacson et al. (1993) require 2340 and $3600 - 4800$ respectively. As computational efforts are proportional to N^2 or N^3, the proposed method significantly reduces the computational storage and time.

For the wave diffraction problem, the proposed method with 1000 panels is compared with the isolated source point method with source points 1500 and 2000. Numerical results show that the proposed method agrees nearly perfect with the method of Beck and King (1989). The isolated source point method with 2000 source points has better agreement than that with 1500 source

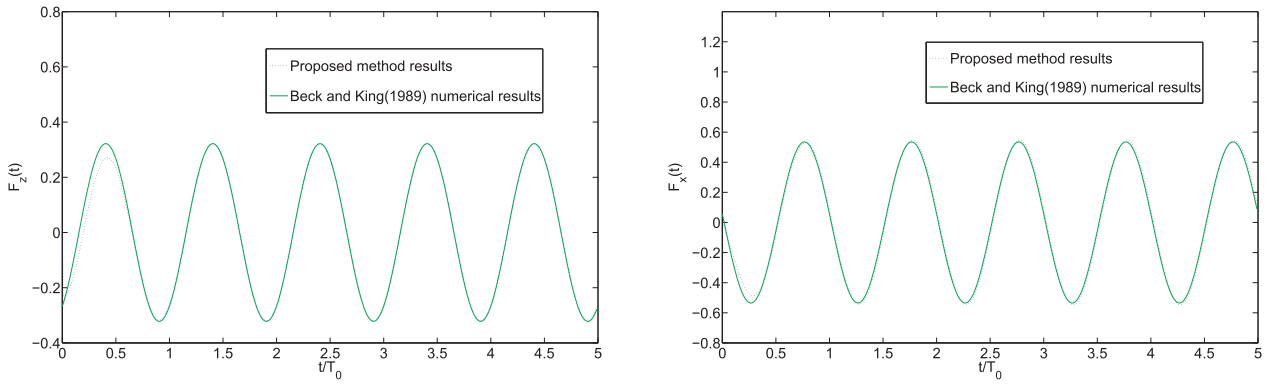

(a) Vertical total diffraction force $F_z(t)$ (b) Horizontal total diffraction force $F_x(t)$

Fig. 13. Comparison of time record of vertical total diffraction force $F_z(t)(a)$ and horizontal total diffraction force $F_x(t)$ (b) between proposed method results and Beck and King (1989) numerical results for a hemisphere subject to a linear incident wave with wave frequency.$kR = 1.0$.

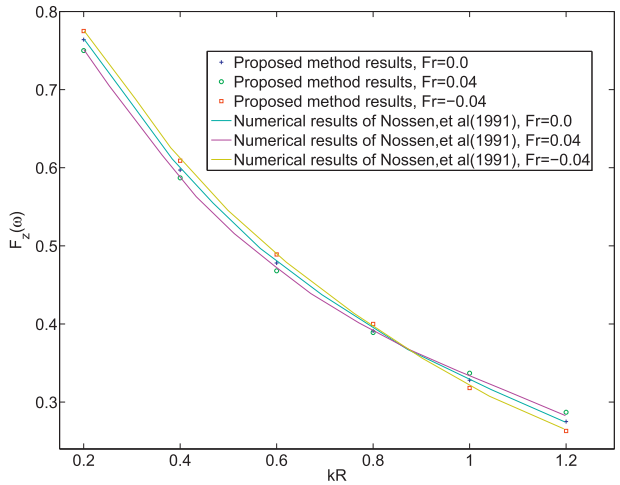

Fig. 14. Comparison of vertical force $F_z(\omega)$ between proposed method results, and numerical prediction of Nossen et al. (1991) for a hemisphere subject to a linear incident wave and current.

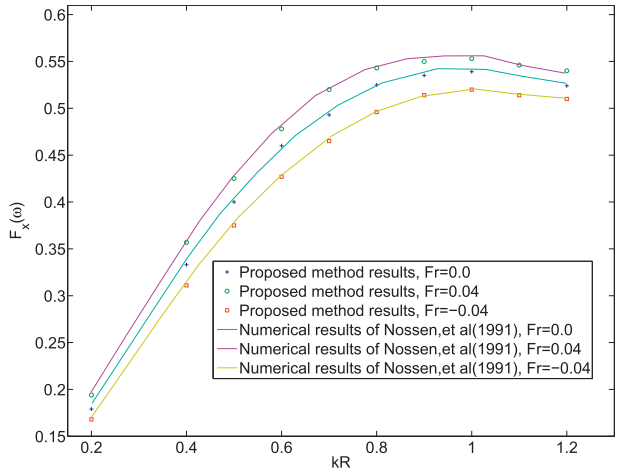

Fig. 15. Comparison of horizontal force $F_x(\omega)$ between proposed method results, and numerical prediction of Nossen et al. (1991) for a hemisphere subject to a linear incident wave and current.

points but it is less closer than the proposed method compared with the results of Beck and King (1989). The proposed method takes about 2 min to finish a $5T_0$ simulation while the other two requires 4 and 8 min in the same computing facility. This numerical case further demonstrates the high accuracy as well as high efficiency of the proposed method. The proposed method was developed to analyze wave-current problem and the comparison demonstrates the wider application of this proposed method.

In this study, linear water wave problems are examined as we only consider small body/wave motion problems. But the proposed method is expected to supply accurate and efficient solution for nonlinear problems as the performance of numerical solution for nonlinear problems largely depends on the solution of linear problems. The nonlinear wave-body interaction problem will be investigated in the future research.

Acknowledgement

The authors gratefully acknowledge the financial support provided by 973 Program of China (2013CB036103, 2015CB251203) and the National Natural Science Foundation of China (Grant No. 51709287).

References

Bai, W., Teng, B., 2013. Simulation of second-order wave interaction with fixed and floating structures in time domain. Ocean Eng. 74, 168–177.
Bandyk, P., Beck, R., 2011. The acceleration potential in fluid–body interaction problems. J. Eng. Math. 70 (1), 147–163.
Bandyk, P.J., 2009. A Body-exact Strip Theory Approach to Ship Motion Computations. Ph.D. thesis. University of Michigan.
Beck, R., 1994. Time-domain computations for floating bodies. Appl. Ocean Res. 16 (5), 267–282.
Beck, R.F., King, B., 1989. Time-domain analysis of wave exciting forces on floating bodies at zero forward speed. Appl. Ocean Res. 11 (1), 19–25.
Cao, Y., Beck, R., Schultz, W., 1993. Numerical computations of two-dimensional solitary waves generated by moving disturbances. Int. J. Numer. Meth. Fluid. 17 (10), 905–920.
Cao, Y., Beck, R.F., 2016. Desingularized boundary integral equations and their applications in wave dynamics and wave–body interaction problems. J. Ocean Eng. Sci. 1 (1), 11–29.
Cao, Y., Schultz, W., Beck, R., 1990. Three-dimensional, unsteady computations of nonlinear waves caused by underwater disturbances. In: Proceedings of the 18th Symposium on Naval Hydrodynamics, vol.1, pp. 417–425.
Cao, Y., Schultz, W., Beck, R., 1991. Three-dimensional desingularized boundary integral methods for potential problems. Int. J. Numer. Meth. Fluid. 12 (8), 785–803.
Chen, Z.-M., 2014. Regular wave integral approach to the prediction of hydrodynamic performance of submerged spheroid. Wave Motion 51 (2), 193–205.
Das, S., Cheung, K.F., 2012. Scattered waves and motions of marine vessels advancing in a seaway. Wave Motion 49 (1), 181–197.

Eatock Taylor, R., Chau, F., 1992. Wave diffraction theorysome developments in linear and nonlinear theory. J. Offshore Mech. Arctic Eng. 114 (3), 185–194.
Feng, A., Chen, Z.-M., Price, W., 2015. A continuous desingularized source distribution method describing wave-body interactions of a large amplitude oscillatory body. J. Offshore Mech. Arctic Eng. 137 (2).
Gao, Z., Zou, Z., 2008. A NURBS-based high-order panel method for three-dimensional radiation and diffraction problems with forward speed. Ocean Eng. 35 (11), 1271–1282.
Hess, J., Smith, A., 1964. Calculation of non-lifting potential flow about arbitrary three dimensional bodies. J. Ship Res. 8 (2), 22–44.
Hulme, A., 1982. The wave forces acting on a floating hemisphere undergoing forced periodic oscillations. J. Fluid Mech. 121, 443–463.
Isaacson, M., Cheung, K.F., 1991. Second order wave diffraction around two-dimensional bodies by time-domain method. Appl. Ocean Res. 13 (4), 175–186.
Isaacson, M., Ng, J.Y., Cheung, K.F., 1993. Second-order wave radiation of three-dimensional bodies by time-domain method. International Journal of Offshore and Polar Engineering 3 (04).
Israeli, M., Orszag, S.A., 1981. Approximation of radiation boundary conditions. J. Comput. Phys. 41 (1), 115–135.
Kim, Y., Kring, D.C., Sclavounos, P.D., 1997. Linear and nonlinear interactions of surface waves with bodies by a three-dimensional rankine panel method. Appl. Ocean Res. 19 (5), 235–249.
Koo, W., Kim, M., 2004. Freely floating-body simulation by a 2D fully nonlinear numerical wave tank. Ocean Eng. 31 (16), 2011–2046.
Koo, W., Kim, M., 2006. Numerical simulation of nonlinear wave and force generated by a wedge-shape wave maker. Ocean Eng. 33 (8), 983–1006.
Koo, W., Kim, M., 2007. Fully nonlinear wave-body interactions with surface-piercing bodies. Ocean Eng. 34 (7), 1000–1012.
Kouh, J., Suen, J., 2001. A 3D potential-based and desingularized high order panel method. Ocean Eng. 28 (11), 1499–1516.
Kring, D.C., Sclavounos, P.D., 1995. Numerical stability analysis for time-domain ship motion simulations. J. Ship Res. 39 (4), 313–320.
Lamb, H., 1945. Hydrodynamics, sixth ed. Dover Publications, Inc, New York, pp. 59–60.
Lee, C., Maniar, H., Newman, J., Zhu, X., 1996. Computations of wave loads using a b-spline panel method. In: Proceedings of the 21st Symposium on Naval Hydrodynamics, pp. 75–92.
Lee, T., 1992. Nonlinear Radiation Problems for a Surface-piercing Body. Ph.D. thesis. University of Michigan.
Lee, T., 2003. Fully nonlinear wave computations for arbitrary floating bodies using the delta method. Int. Hydrodyn. 15 (002).
Maniar, H.D., 1995. A Three Dimensional Higher Order Panel Method Based on B-splines. Ph.D. thesis. Massachusetts Institute of Technology.
Nakos, D., Sclavounos, P., 1990. On steady and unsteady ship wave patterns. J. Fluid Mech. 215, 263–288.
Nossen, J., Grue, J., Palm, E., 1991. Wave forces on three-dimensional floating bodies with small forward speed. J. Fluid Mech. 227, 135–160.
Sclavounos, P.D., Nakos, D.E., 1988. Stability analysis of panel methods for free-surface flows with forward speed. In: Proceeding of the 17th Symposium on Naval Hydrodynamics.
Tanizawa, K., 1996. Long time fully nonlinear simulation of floating body motions with artificial damping zone. J. Soc. Nav. Archit. Jpn. 180, 311–319.
Wang, L., Tang, H., Wu, Y., 2015. Simulation of wave–body interaction: a desingularized method coupled with acceleration potential. J. Fluid Struct. 52, 37–48.
Wang, L., Tang, H., Wu, Y., 2016. Wave interaction with a surface-piercing body in water of finite depth: a parametric study. Eng. Appl. Comput. Fluid Mech. 10 (1), 512–528.
Wehausen, J., Laitone, E., 1960. Surface Waves. Springer.
Yonghui, L., Xinsen, L., 1988. Polar coordinate transformation approach for treatment of singular integrals in boundary element methods. Appl. Math. Mech. 9 (10), 959–967.
Zhang, X., Bandyk, P., Beck, R., 2010. Time-domain simulations of radiation and diffraction forces. J. Ship Res. 54 (2), 79–94.
Zhang, X., Beck, R., 2007. Computations for large-amplitude two-dimensional body motions. J. Eng. Math. 58 (1), 177–189.
Zhang, X., Beck, R., 2008. Three-dimensional large amplitude body motions in waves. J. Offshore Mech. Arctic Eng. 130 (4), 16–23.
Zhang, X., Khoo, B., Lou, J., 2006. Wave propagation in a fully nonlinear numerical wave tank: a desingularized method. Ocean Eng. 33 (17), 2310–2331.